The Astronomical Journal, 148:62 (13pp), 2014 October doi:10.1088/0004-6256/148/4/62

THE HD 5980 MULTIPLE SYSTEM: MASSES AND EVOLUTIONARY STATUS

Gloria Koenigsberger[1,2], Nidia Morrell[3], D. John Hillier[4], Roberto Gamen[5], Fabian R. N. Schneider[6],
Nicolás González-Jiménez[6], Norbert Langer[6], and Rodolfo Barbá[7]
[1] Instituto de Ciencias Físicas, Universidad Nacional Autónoma de México, Ave. Universidad S/N, Cuernavaca, Morelos 62210, México
[2] Instituto de Astronomía, Universidad Nacional Autónoma de México, Apdo. Postal 70-264, México D.F. 04510, México; gloria@astro.unam.mx
[3] Las Campanas Observatory, The Carnegie Observatories, Colina El Pino s/n, Casillas 601, La Serena, Chile; nmorrell@lco.edu
[4] Department of Physics and Astronomy, and Pittsburgh Particle Physics, Astrophysics and Cosmology Center (PITT PACC), 3941 O'Hara Street,
University of Pittsburgh, Pittsburgh, PA 15260, USA; hillier@pitt.edu
[5] Facultad de Ciencias Astronómicas y Geofísicas, Universidad Nacional de La Plata, and Instituto de Astrofísica de La Plata (CCT La Plata-CONICET),
Paseo del Bosque S/N, B1900FWA La Plata, Argentina; rgamen@fcaglp.unlp.edu.ar
[6] Argelander-Institut für Astronomie, Auf dem Hügel 71, D-53121 Bonn, Germany; fschneid@astro.uni-bonn.de,
ngonzalez@astro.uni-bonn.de, nlanger@astro.uni-bonn.de
[7] Departamento de Física, Av. Juan Cisternas 1200 Norte, Universidad de la Serena, La Serena, Chile; rbarba@dfuls.cl

Received 2013 December 4; accepted 2014 June 15; published 2014 September 3

ABSTRACT

New spectroscopic observations of the LBV/WR multiple system HD 5980 in the Small Magellanic Cloud are used to address the question of the masses and evolutionary status of the two very luminous stars in the 19.3 day eclipsing binary system. Two distinct components of the N v 4944 Å line are detected in emission and their radial velocity variations are used to derive masses of 61 and 66 $M_\odot$, under the assumption that binary interaction effects on this atomic transition are negligible. We propose that this binary system is the product of quasi-chemically homogeneous evolution with little or no mass transfer. Thus, both of these binary stars may be candidates for gamma-ray burst progenitors or even pair instability supernovae. Analysis of the photospheric absorption lines belonging to the third-light object in the system confirm that it consists of an O-type star in a 96.56 day eccentric orbit ($e = 0.82$) around an unseen companion. The 5:1 period ratio and high eccentricities of the two binaries suggest that they may constitute a hierarchical quadruple system.

Key words: binaries: eclipsing – stars: evolution – stars: individual (HD 5980) – stars: massive – stars: Wolf–Rayet

Online-only material: color figures

1. INTRODUCTION

Massive stars play an important role in the chemical evolution of galaxies and in shaping the interstellar medium. They are found in regions of recent star formation and near the Galactic center, and they are associated with fascinating phenomena such as the formation of neutron stars and black holes. But despite their importance, there are still gaps in our understanding of their structure and evolution. One of these gaps involves the manner in which they reach the final stages of evolution and explode as supernovae (SNe). In particular, there is great uncertainty concerning the amount of mass that is lost in the post-main sequence evolutionary stages, thus leading to uncertainties in the stellar structure prior to the final SN event. Central to this issue is the role played by the Luminous Blue Variables (LBV).

According to current evolutionary scenarios, classical LBVs are stars in transition from the main sequence to the Wolf–Rayet (WR) stage and they are in the process of shedding their outer layers to expose the products of the CNO nuclear reactions taking place in their centers (Maeder & Meynet 1987; Langer et al. 1994, Langer 2012). Enhanced mass-loss rates are observed to occur during the maxima of the variability cycles when up to $\sim$10 $M_\odot$ can be ejected, as illustrated by η Carinae's mid-19th century event (Humphreys & Davidson 1994). However, the underlying processes that cause the LBV instability are unknown (see, for example, Vink et al 2012). Thus, a crucial ingredient in the models of massive star evolution is missing. This problem is compounded by the fact that the current mass of the LBVs is in general poorly constrained.

The Small Magellanic Cloud (SMC) harbors an LBV eclipsing binary that has been studied since the 1950s and which underwent a major eruption in 1994. It has the highest luminosity of all the well-studied LBVs, except perhaps for η Carinae, and also shares with η Car the exceptional characteristic of showing a WR type spectrum. Furthermore, both systems are associated with massive and young stellar clusters, HD 5980 lying in the periphery of NGC 346. Its wind properties and many of its fundamental parameters have been derived in a series of studies based on *IUE*, *HST*/STIS, and optical observations (Perrier et al. 2009; Georgiev et al. 2011; Foellmi et al. 2008; Koenigsberger 2004; Koenigsberger et al. 2010). The mass determinations so far, however, have a large degree of uncertainty, a problem we address in this investigation. In addition, the long baseline of data now available allows a re-assessment of the nature of the third component of the system, which we now can confirm consists of a binary system.

The organization of this paper is as follows. In Section 2 we review the characteristics of the HD 5980 system; in Sections 3 and 4 we describe, respectively, the observational data and the radial velocity (RV) measurements; Section 5 presents the orbital solutions; in Section 6 we discuss the evolutionary paths that may explain HD 5980's current state; and in Section 7 we summarize the conclusions.

2. DESCRIPTION OF THE HD 5980 SYSTEM

The spectrum of HD 5980 is the sum of several components. Most prominent are the two emission-line stars belonging to the close eclipsing binary system ($P_{\rm AB} = 19.3$ days). Following the

Table 1
Low Dispersion LCO Spectra

Year	Telescope	Instrument	HJD −2,450,000	Phase 19.26 days
2009	Baade Mag 1	IMACS	4900.496	0.476
2009	Baade Mag 1	IMACS	4902.494	0.579
2009	Baade Mag 1	IMACS	5072.798	0.419
2009	Clay Mag 2	MagE	5140.702	0.944
2009	Clay Mag 2	MagE	5142.508	0.038
2009	Clay Mag 2	MagE	5143.504	0.089
2010	Clay Mag 2	MagE	5527.770	0.035

Table 2
High Dispersion LCO Spectra

Year	Telescope	Instrument	HJD −2,450,000	Phase 19.2654 days
2006	DuPont	Echelle	3920.861	0.626
2007	Clay Mag 2	MIKE	4342.731	0.524
2008	DuPont	Echelle	4670.799	0.553
2008	DuPont	Echelle	4671.823	0.606
2008	DuPont	Echelle	4672.799	0.656
2008	Clay Mag 2	MIKE	4774.800	0.951
2009	Clay Mag 2	MIKE	5161.687	0.033
2010	Clay Mag 2	MIKE	5205.520	0.308
2010	DuPont	Echelle	5341.902	0.387
2010	DuPont	Echelle	5342.889	0.439
2010	DuPont	Echelle	5480.501	0.581
2010	DuPont	Echelle	5481.756	0.646
2010	DuPont	Echelle	5482.811	0.702
2010	DuPont	Echelle	5506.500	0.931
2010	DuPont	Echelle	5507.542	0.985
2010	DuPont	Echelle	5508.508	0.035
2010	DuPont	Echelle	5509.500	0.087
2010	DuPont	Echelle	5510.521	0.140
2010	DuPont	Echelle	5511.546	0.193
2010	DuPont	Echelle	5512.502	0.243
2011	Clay Mag 2	MIKE	5761.866	0.186
2011	DuPont	Echelle	5844.530	0.477
2011	DuPont	Echelle	5845.564	0.530
2011	DuPont	Echelle	5846.620	0.585
2012	Clay Mag 2	MIKE	6084.887	0.953
2012	DuPont	Echelle	6120.766	0.815
2013	DuPont	Echelle	6496.804	0.334
2013	DuPont	Echelle	6497.804	0.385
2013	DuPont	Echelle	6498.833	0.440
2013	DuPont	Echelle	6501.750	0.592
2013	DuPont	Echelle	6502.754	0.643
2013	DuPont	Echelle	6533.737	0.252

convention introduced by Barbá et al. (1996), the star "in front" at orbital phase $\phi = 0.00$ is labeled *Star A* and its companion is labeled *Star B*. In addition, there is a third component, *Star C*, whose photospheric absorptions remain stationary on the 19.3 day orbital timescale and which contributes a significant fraction of the observed light (Breysacher & Perrier 1991; Niemela 1988; Koenigsberger et al. 2002; Perrier et al. 2009).

HD 5980's emission-line spectrum is highly variable on orbital and decade-long timescales. The short-timescale variability is produced by the periodic Doppler motion of the emission lines that are formed in the winds of *Stars A* and *B* combined with binary interaction effects, among which the ones that are most likely dominant are irradiation, wind–wind collisions (WWCs) and wind eclipses. Different lines are affected to a different degree, depending on their transition probabilities and formation mechanisms. The long-term variation is due to *Star A*'s changing wind structure, which appears to be triggered by variations in the hydrostatic radius (Koenigsberger et al. 1998; and Georgiev et al. 2011).

Star B is thought to be a WN4 star (Breysacher et al. 1982; Niemela 1988), and hence it has a stellar wind that contributes significantly to the emission-line spectrum. Traces of its broad UV emission lines can be seen underlying the narrow emissions that appeared during the 1994 eruptive event (see Koenigsberger 2004, Figure 11). Furthermore, the shape of the eclipse light curve observed in the late 1970s leads to the conclusion that *Star B* possesses an extended occulting region having a radius of 0.269a, where a is the semi-major axis of the orbit (Perrier et al. 2009). Both of these facts lend credence supporting the view that *Star B* is a WNE-type star.

The spectrum of *Star C* is that of an O-type supergiant. Its optical spectrum is dominated by H-Balmer, He I, and other low-ionization photospheric absorption lines, while in the UV it presents a modest P Cygni Si IV 1400 Å profile (Georgiev et al. 2011). The RV of the O III 5592 Å photospheric line was found to display a periodic behavior with $P_C \sim 97$ days, and the solution to this RV curve yielded a highly eccentric $e \sim 0.8$ orbit, leading to the conclusion that *Star C* is also a binary system (Schweickhardt 2000).

The determination of the masses of the individual components in the system is a challenging problem due to the very broad and variable emission lines. Using photographic spectra obtained during 1981–1983, Niemela (1988) estimated masses $M_A \sim 46\,M_\odot$ and $M_B \sim 43\,M_\odot$ for *Star A* and *B*, respectively. Foellmi et al. (2008) analyzed high dispersion spectra obtained in 1998, 1999, and 2005 and concluded that, if the observed line profiles can be interpreted as being formed primarily in the winds of *Star A* and *Star B* (as opposed to in the WWC region; see Section 5.3), then the measured RV variations implied $M_A \sim$ 58–79 $M_\odot$ and $M_B \sim$ 51–67 $M_\odot$. The stellar wind analysis performed by Georgiev et al. (2011) led to the conclusion that for a stable solution connecting the photosphere with the stellar wind to be possible, $M_A \geqslant 90\,M_\odot$. Moffat et al. (1998) assumed that at least part of the photospheric absorptions in the spectrum arise in *Star A*, from which they derived masses $M_A \sim$ 28–38 $M_\odot$ and $M_B \sim$ 6–18 $M_\odot$. A possible explanation for the modulation on the 19.3 day period of the absorption lines claimed by Moffat et al. (1998) was put forth by Georgiev & Koenigsberger (2004). They showed that if *Star A* is a rapid rotator, the superposition of its broad and shallow photospheric lines could produce a slight RV fluctuation in *Star C*'s sharper lines and lead to the false conclusion that they follow the 19.3 day orbital period, albeit with a very small RV curve amplitude.

3. OBSERVATIONAL MATERIAL

The observations of HD 5980 analyzed in this paper were obtained at Las Campanas Observatory and consist of seven low dispersion spectra obtained with the 6.5 m Magellan telescopes in 2009 and 2010; 25 echelle spectra obtained with the du Pont telescope between 2006 and 2013; and six spectra obtained on the 6.5 Clay Magellan telescope between 2007 and 2012. Tables 1 and 2 list the year the spectrum was obtained, the telescope and instruments used, Heliocentric Julian Date of observation, and orbital phase for $P = 19.2654$ days and $T_0 =$ HJD 2,443,158.705 (Sterken & Breysacher 1997).

The Baade 6.5 m (Magellan-I) low dispersion spectra were obtained with IMACS in its long camera mode (*f*4) with a 600 line mm^{-1} grating that provided spectral coverage from roughly 3700 to 6800 Å at a spectral resolution of 1.4–1.5 Å ($R \sim 4000$). One of these spectra was described in Koenigsberger et al. (2010). The Clay 6.5 m (Magellan-II) low dispersion spectra were obtained with the Magellan Echellette (MagE) using the 1″ slit providing a spectral resolution of 1 Å. Thirteen echelle orders were extracted covering the wavelength region from 3130 Å to 9400 Å. The signal-to-noise ratio (S/N) ranges from 100 to 200 for a single 150 s exposure. The usual ThAr comparison lamp was used for wavelength calibration, and the data were reduced using an adaptation of the *mtools* package, available for the reduction of Magellan Inamori Kyocera Echelle (MIKE) spectra (see below) in combination with *IRAF*[8] echelle routines for the reduction of MIKE spectra.[9] Spectra of spectrophotometric standard stars observed during the same nights of observation were used to derive a sensitivity function. The individual flux calibrated echelle orders were then normalized and merged in the final spectrum. One of these MagE observations was already described in Georgiev et al. (2011).

The high resolution du Pont telescope spectra were obtained with the echelle spectrograph and a 1″ slit. The spectral resolution of these data ranges from 0.15 to 0.22 Å ($R \sim 25{,}000$) and the wavelength coverage goes from 3500 to 8800 Å.

The high resolution Clay (Magellan-II) spectra were obtained with the MIKE spectrograph using a 0.″7 slit and applying a 2×2 binning to both blue and red detectors. This configuration results in a spectral resolution of ∼34,000 (FWHM ranging from 0.10 to 0.25 Å). Reductions were carried out with the specially designed *IRAF* scripts contained in the *mtools* package developed by Jack Baldwin and available at the Las Campanas web site. The reduced spectra were flux calibrated using spectra of spectrophotometric standards obtained during the same observing nights.

In addition to the new spectra described above, we used data obtained in 1998, 1999, 2005, and 2006 with FEROS on the 2.2 m MPI telescope at La Silla Observatory, previously described in Kaufer et al. (2002), Schweickhardt (2000), and Foellmi et al. (2008).

4. RADIAL VELOCITIES AND ORBITAL SOLUTIONS

In the following sections we will describe the procedure followed for obtaining the RV curves of the two emission-line objects and of the star responsible for the absorption lines. For this, it is useful to keep in mind that the eclipses of the 19.3 day binary occur at $\phi = 0.00$ (*Star A* "in front") and $\phi = 0.36$ (*Star B* "in front") and maximum receding velocity of *Star A* is at $\phi \sim 0.1$.

4.1. Emission Lines

Figure 1 shows the spectra obtained in 2009 at orbital phases $\phi = 0.038$ and 0.944 in the $\lambda\lambda$3100–7400 wavelength region. The dominant features are emission lines of He II, N IV, N V, and C IV; He I is weakly present in emission at λ5875.

All the major emission lines undergo prominent shape changes over the orbital cycle, similar to those found in previous optical data sets (Breysacher et al. 1982; Breysacher & François 2000; Moffat et al. 1998; Foellmi et al. 2008; Koenigsberger et al. 2010). The dominant type of variability involves the FWHM intensity which systematically is greater at elongations than at eclipses. *Star A* and *Star B* are believed to possess stellar winds of similar ionization characteristics and the orbital motion of these stars combined with the interactions and the eclipses produces the FWHM variations. In Section 5.3 we discuss the validity of this assumption in the light of the various interaction effects that are present in the *Star A* + *Star B* system, and we argue in favor of the possibility of using the weaker high ionization emission lines for deriving the orbital parameters. Because the ionization rapidly decreases outward, the bulk of their emission arises in the innermost regions of the wind and are thus less sensitive to external perturbations.

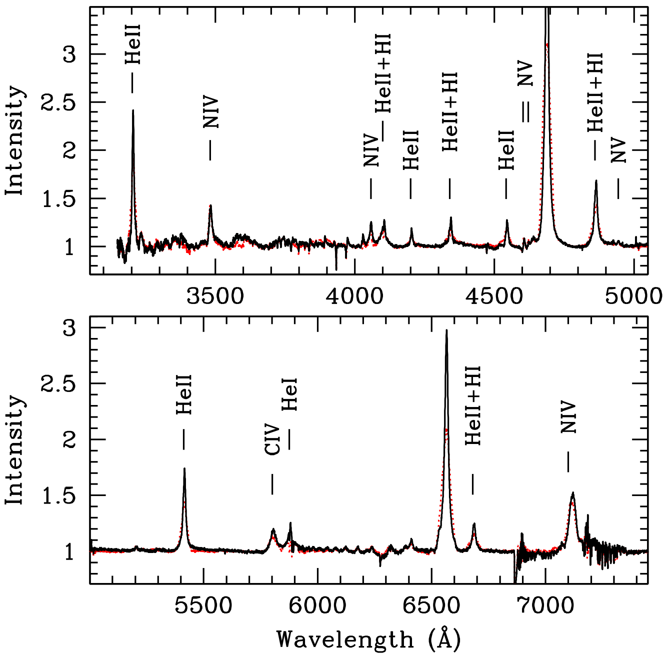

Figure 1. Overview of the optical spectrum in 2009 at orbital phases 0.038 and 0.944 (dots). At $\phi = 0.038$, most emission lines have larger line-to-continuum ratios due in part to the eclipse of *Star B* by *Star A*.

(A color version of this figure is available in the online journal.)

Narrow lines are also the best ones to measure on the echelle spectra, where uncertainties in the rectification of the individual orders represents a challenge for accurate measurement of very broad and variable emissions. In addition, it is advisable to select lines that lie near the center of the order where the S/N is greatest and that are not blended with other lines. We found that the line that is best suited for the RV curve analysis is N V 4944 Å. This is one of the three N V lines that lie in the same echelle order at $\lambda\lambda$4944.37, 4932.00, and 4952.07. The first of these lies closest to the center of the order in most of our spectra and it is the only one of these three lines that is clearly visible. This is consistent with its intensity in our *Star A* CMFGEN model, where it has an equivalent width ∼8 times greater than that of λ4932 and 4952.

Figure 2 displays the rectified[10] echelle orders containing these N V transitions and stacked from bottom to top with increasing orbital phase plotted on a velocity scale corrected for an assumed SMC systemic velocity of +150 km s^{-1}. It shows that N V 4944 Å splits into two components during the phase intervals: 0.09–0.24 (when *Star A* is receding from the observer) and 0.58–0.81 (when it is approaching). A similar pattern is

---

[8] *IRAF* is written and supported by the National Optical Astronomy Observatories (NOAO) in Tucson, Arizona. NOAO is operated by the Association of Universities for Research in Astronomy (AURA), Inc. under cooperative agreement with the National Science Foundation.

[9] *mtools* package: http://www.lco.cl/telescopes-information/magellan/instruments/mike/iraf-tools.

[10] The echelle orders were rectified by tracing the continuum level on each order and then using the resulting curve for the normalization.

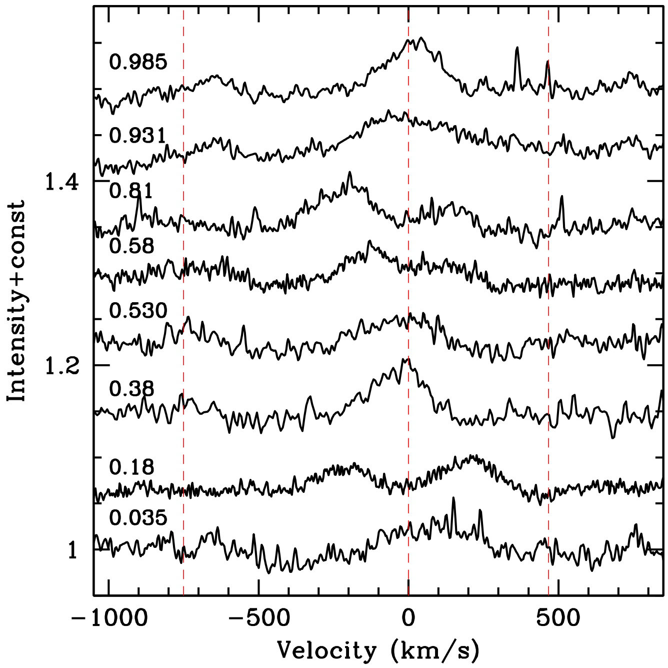

Figure 2. Montage of selected N v 4944 line profiles from the LCO echelle data covering the 19.3 day orbital cycle, plotted on a velocity scale corrected for an assumed local SMC velocity of +150 km s^{-1}. *Star A* occults *Star B* at $\phi = 0$, and approaches the observer at $\phi = 0.81$. Orbital phases with two digits only after the decimal point indicate spectra that have been averaged over phase. Spectra are shifted vertically for clarity. The dotted lines indicate the rest wavelength location of the weaker neighboring N v lines.

(A color version of this figure is available in the online journal.)

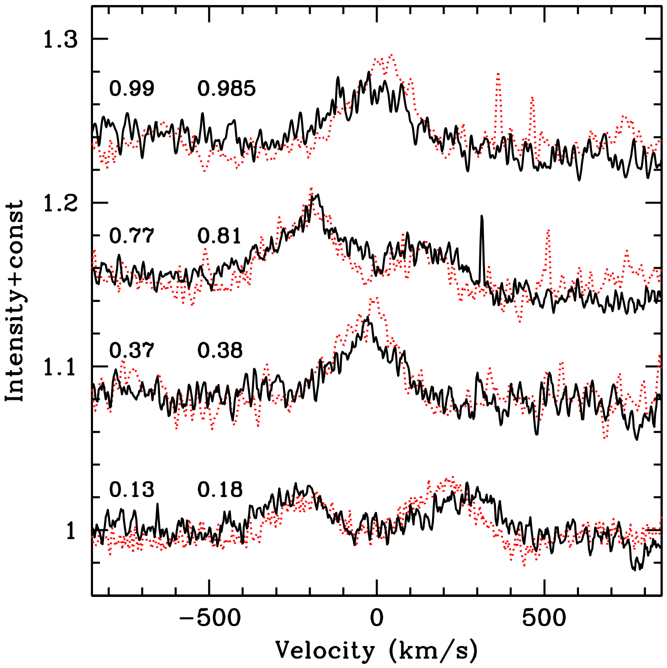

Figure 3. Montage of the N v 4944 Å line in the 2005–2006 FEROS spectra showing the same behavior as observed in the 2009–2011 LCO data. The dotted spectra are the same LCO spectra as plotted in Figure 2. The orbital phases for FEROS (left) and LCO (right) are indicated. The velocity scale is corrected for the adopted systemic SMC velocity of +150 km s^{-1}.

(A color version of this figure is available in the online journal.)

also observed to occur in the FEROS data of 2005–2006, as illustrated in Figure 3.

The RVs of N v 4944 were measured with a two-Gaussian deblending routine in *IRAF*. These measurements were first performed on the non-rectified LCO echelle orders and then repeated on the rectified orders. In the spectra in which the two components are well separated, the largest uncertainty is ~10 km s^{-1} and stems from the definition of the continuum level. At eclipse phases where only one centrally located emission is visible, the measured RV is assigned to the uneclipsed component, with the uncertainty stemming also from the continuum level. When the lines are not well separated, the uncertainty can be as large as ~30 km s^{-1}.

Consistent measurements were not possible on a number of spectra due in general to a combination of too poor S/N, spurious features, and cosmic ray hits, and these spectra have been excluded from the N v 4944 analysis. The 2005–2006 FEROS exposures were performed in pairs, and each individual spectrum was measured and the results averaged. The results are presented in Table 3 and Figure 4.

We searched for other N v lines that could be measured in a similar fashion as N v 4944, but they are all either too weak or lie too close to the edges of the orders, except for λλ4603–19 which, however, possess strong overlapping P Cygni absorption components which do not allow reliable measurements.

Another line that is amenable for measurement is N iv 4057 Å. It was measured by Foellmi et al. (2008) in the 1999 and 2005 FEROS spectra by assuming that it consists of two components that are Doppler-shifted due to orbital motion. We have applied the same procedure to measure this line in the LCO spectra listed in Table 2. To do so, we fixed the limits for the deblending routine at ±500 km s^{-1}, which therefore neglects the broad emission-

Table 3
Radial Velocity Measurements of N v 4944

HJD[a]	Phase[b]	A[c]	B[c]	HJD[a]	Phase[b]	A[c]	B[c]
LCO				FEROS			
4671.823	0.606	14	301	1375.922	0.527	32	...
4672.799	0.656	15	344	1380.898	0.786	−90	301
5341.897	0.380	...	123	1381.902	0.838	...	266
5342.889	0.439	111	...	1388.840	0.198	314	−85
5481.756	0.646	−17	311	1389.883	0.252	306	−15
5482.811	0.702	−57	319	1390.828	0.301	160	43
5506.500	0.931	78	193	1391.832	0.353	...	65
5507.542	0.985	152	...	1392.828	0.405	...	89
5508.508	0.035	259	7	1393.871	0.459	...	95
5509.500	0.087	343	−75	1394.891	0.512	35	...
5510.521	0.140	386	−142	3538.885	0.799	13	306
5512.502	0.243	339	−61	3541.894	0.955	113	...
5761.866	0.186	360	−56	3561.877	0.992	117	...
5844.530	0.477	−17	151	3576.798	0.767	−98	322
5845.564	0.530	−4	166	3635.510	0.814	−47	294
5846.620	0.585	6	242	3638.763	0.983	128	...
6120.767	0.810	−60	283	3641.663	0.133	399	−110
6496.804	0.334	...	146	3665.535	0.373	...	94
6497.804	0.385	...	139	3715.798	0.982	78	...
6498.833	0.440	...	178	3716.536	0.020	133	...
6501.750	0.592	89	282	3731.546	0.799	−59	289
6502.754	0.643	9	302	3734.615	0.959	71	...
6533.737	0.252	356	−22	3735.553	0.007	126	...
				3738.544	0.162	369	−115

Notes.
[a] HJDs are −2,450,000.
[b] Phases were computed with $P = 19.2654$ days.
[c] RVs are given in units of km s^{-1}, and include the heliocentric correction.

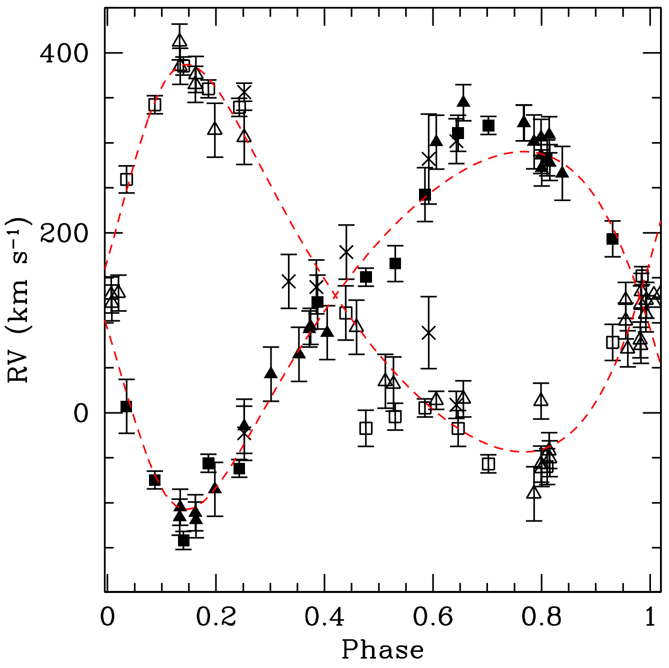

Figure 4. Radial velocities of the N v 4944 Å emission line obtained in 1999–2008 (triangles), 2009–2012 (squares), and 2013 (crosses) plotted as a function of the 19.2654 day orbital phase. Error bars indicate the measurement uncertainties. The dash curves correspond to the orbital solution listed in Table 6 with a systematic shift of -20 km s^{-1}.

(A color version of this figure is available in the online journal.)

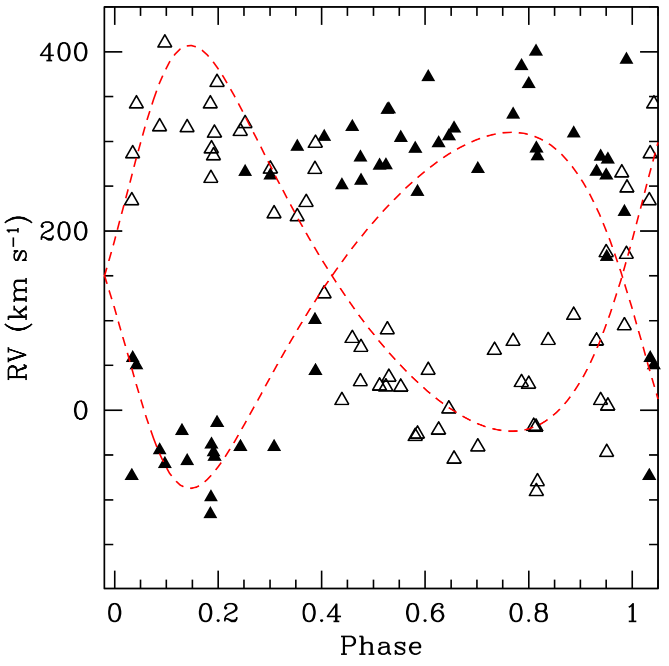

Figure 5. Radial velocity measurements of the N iv 4057 emission line from the rectified LCO orders and from the archival FEROS data plotted as a function of the 19.2654 day orbital phase. Open and filed-in symbols correspond, respectively, to *Star A* and *Star B*. The larger dispersion here compared to the plot of N v 4944 Å is most likely related to stronger interaction effects in this N iv emission line.

(A color version of this figure is available in the online journal.)

line wings. The resulting RVs of the LCO and FEROS data sets are plotted in Figure 5, which shows that the RV variations of this line are similar to those found for N v 4944 Å. There is, however, a systematic difference in the LCO and FEROS RV curves of N iv 4057 Å at orbital phases 0.25–0.45, most likely a consequence of epoch-dependent variations in *Star A*'s wind structure.[11]

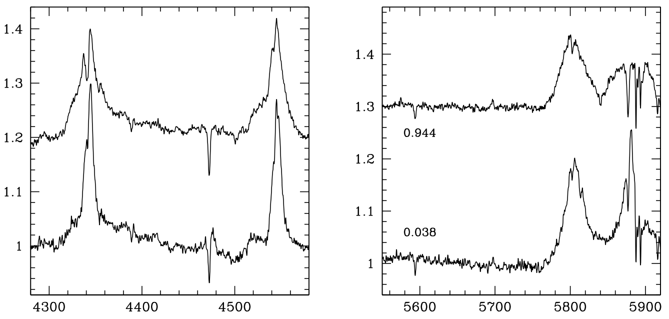

Figure 6. Selected spectral regions showing photospheric absorption from *Star C* in the low dispersion spectra obtained at orbital phases $\phi_{\rm AB} = 0.038$ (lower tracing) and 0.944 (upper tracing; displaced vertically for clarity). Shown are He i 4387 and 4471 Å (left panel) and O iii 5592, C iv 5801, 5812, and He i 5875 Å (right panel).

4.2. Photospheric Absorption Lines

It is now well-established that the sharp photospheric absorptions arise in *Star C*, but the presence of such absorptions arising in *Star A* and/or *Star B* cannot be excluded. A search for photospheric absorptions has repeatedly been conducted (Niemela 1988; Koenigsberger et al. 2002) with no success. This can be explained if the optical depth of the stellar wind is too large for the spectrum of the hydrostatic radius to be visible, an explanation that is supported by the CMFGEN model which indicates that the optical depth at the sonic radius is ∼1.8 (Georgiev et al. 2011; model fit to the 2009 spectra). However, there is evidence that the wind is becoming weaker so that photospheric absorptions may be expected to become visible, prompting a new search in the current data set.

Ten of the du Pont Telescope observations were obtained over a 32 night timespan in 2010 and cover the orbital phases 0.58–1.24. We first searched these spectra for photospheric absorption lines with RV variations that would allow them to be associated with either *Star A* or *Star B*. Although many potential identifications were made, we were unable to convincingly find any one feature that appears in several spectra with RV shifts that would prove that it arises in one of these stars. The search was then extended to the other spectra with similar inconclusive results. It is worth noting that photospheric absorptions in a rapidly rotating star are difficult to detect in general and more so if they are superposed on broad and variable emission lines as might be the case for *Star A* and/or *Star B*.

We now shift our focus to the photospheric absorptions that are visible in the spectra and do not partake in the 19.3 day orbit. These include the H-Balmer series out to H20, as well as prominent He i 4471, 5875 Å, O iii 5592 Å, and C iv 5806, 5812 Å, and weaker absorption attributable to He ii 4542 and 5411 Å. The absorptions are most clearly visible at orbital phases when the underlying emissions are broadest (such as at $\phi = 0.944$ in Figure 6). As mentioned previously, the O iii 5592 Å line was shown to undergo RV variations consistent with a $P_C \sim 96.5$ days, $e \sim 0.8$ orbit (Schweickhardt 2000).

---

[11] In this phase interval *Star B* is "in front" of the companion, and changes in the wind structure of *Star A* would affect the geometry of the wind–wind collision region; however, given the larger *Star A* wind density, the irradiation effects would also be more important and back-scattered emission would contribute to the "blue" emission-line wing.

Table 4

LCO Radial Velocity Measurements for *Star C*

HJD −2,450,000	Phase 19.2654 days	Phase 96.56 days	λ5592a km s^{-1}	λ4471a km s^{-1}	λ5875a km s^{-1}	λ5696e km s^{-1}
3920.861	0.626	0.350	. . .	191	192	. . .
4342.731	0.524	0.719	. . .	139	150	. . .
4670.799	0.553	0.116	215	209	216	203
4671.823	0.606	0.127	191	208	210	198
4672.799	0.657	0.137	192	198	202	190
4774.800	0.951	0.193	183	. . .	183	174
5161.687	0.033	0.200	186	177	168	169
5205.520	0.308	0.654	148	138	134	135
5341.902	0.388	0.067	245	227	250	. . .
5342.889	0.439	0.077	225	220	239	. . .
5480.501	0.582	0.502	175	159	149	159
5481.756	0.647	0.515	170	170	172	121
5482.811	0.702	0.526	167	160	160	180
5506.500	0.931	0.771	118	137	122	115
5507.542	0.985	0.782	133	132	131	122
5508.508	0.035	0.792	127	105	117	128
5509.500	0.087	0.802	128	114	116	122
5510.521	0.140	0.813	127	110	106	115
5511.546	0.193	0.823	110	109	101	117
5512.502	0.243	0.833	111	112	99	114
5761.866	0.186	0.416	186	171	171	177
5844.530	0.477	0.272	189	185	193	184
5845.564	0.531	0.283	187	186	193	141
5846.620	0.586	0.293	172	176	184	136
6084.887	0.953	0.761	174	156	154	144
6120.766	0.815	0.133	193	204	214	184
6496.804	0.334	0.027	216	213	228	203
6497.787	0.385	0.037	233	211	219	. . .
6498.833	0.440	0.048	212	204	218	. . .
6501.750	0.591	0.078	232	216	216	238
6502.754	0.643	0.089	239	217	213	. . .
6533.737	0.252	0.409	195	189	197	197

We selected He I 4471 and 5875 Å and O III 5592 Å for measurement, all of which are relatively uncontaminated by neighboring lines and lie at reliable locations within the echelle orders. In addition, we measured the C III 5696 Å emission line. Tables 4 and 5 list the RVs obtained by fitting Gaussians to the cores of the lines in the LCO and the FEROS spectra, respectively, and Figure 8 displays these values as a function of phase computed with the two periods: $P_{\rm AB} = 19.2654$ days (top panels) and $P_C = 96.56$ days. All RVs follow a clear periodic trend with P_C, as shown in the bottom panels, where data from 2005–2012 (left) and from 1998–1999 (right) are plotted.[12] Both of these RV sets are combined in Figure 7 illustrating a clear minimum at $\phi_C \sim 0$ and maximum at $\phi_C \sim 0.05$, consistent with Schweickhardt's conclusion that *Star C* is a binary.

It is a curious coincidence that $P_C = 5 \times P_{\rm AB}$, which leaves the lingering suspicion that perhaps the data are really only modulated with $P_{\rm AB}$ but that the 1998–1999 activity levels of *Star A* prevented this modulation from being uncovered.[13] Thus, we revisited this issue and plotted the 2010–2012 LCO RVs as a function of phase using $P_{\rm AB}$ (Figure 8, top left panel), finding a clear modulation with this period. However, upon closer inspection, we find that the 2010–2012 spectra are clustered by chance in the two phase intervals $\phi_C =$ 0.0–0.3 and 0.7–1.0, which correspond, respectively, to times of maximum and minimum RVs. This is shown by plotting with different symbols the data in each of these two phase intervals in the top left panel of Figure 8. This serves as a cautionary tale to be heeded when finding modulations in data sets that incompletely sample the actual period. Furthermore, if we now plot the LCO data from observations prior to 2010 together with the 1998–1999 data, the plot becomes a scatter diagram as found by Schweickhardt (2000) for the 1998–1999 observations. Hence, we conclude that P_C does indeed exist and can only be associated with *Star C* unless *Star A* or *Star B* undergo some kind of pulsation cycle on the P_C timescale which also masks the RV variations on $P_{\rm AB}$, something we do not consider very likely.

Table 5

FEROS Radial Velocity Measurements for *Star C*

HJD −2,450,000	Phase 19.2654 days	Phase 96.56 days	λ5592a km s^{-1}	λ4471a km s^{-1}	λ5875a km s^{-1}	λ5696e km s^{-1}
1094.797	0.935	0.082	251	183	. . .	. . .
1100.773	0.245	0.144	214	208	189	189
1133.691	0.954	0.485	205	192	132	. . .
1138.512	0.204	0.535	166	141	128	. . .
1145.547	0.569	0.608	. . .	198	. . .	174
1150.508	0.827	0.659	181	201	61	. . .
1174.523	0.073	0.908	. . .	126	91	. . .
1176.555	0.179	0.929	82	108	87	. . .
1181.516	0.436	0.980	80	. . .	. . .	11
1183.523	0.541	0.001	122:	111:	. . .	154
1185.562	0.646	0.022	. . .	229	. . .	94:
1187.523	0.748	0.043	. . .	234	236	194
1189.516	0.852	0.063	. . .	232	. . .	. . .
1191.516	0.955	0.084	. . .	268	. . .	. . .
1193.531	0.060	0.105	217	216	. . .	204
1197.535	0.268	0.146	. . .	227	. . .	. . .
1374.918	0.475	0.983	68	69	44	-14
1375.922	0.527	0.994	88	88	70	56
1379.902	0.734	0.035	222	247	. . .	. . .
1381.902	0.838	0.056	212	219	. . .	211
1382.852	0.887	0.066	200	216	260	170
1383.855	0.939	0.076	186	222	245	127
1384.809	0.989	0.086	195	240	208	214
1386.891	0.097	0.107	180	216	. . .	226
1388.840	0.198	0.128	172	239	. . .	181
1389.883	0.252	0.138	184	216	216	159
1390.828	0.301	0.148	178	207	224	206
1392.828	0.405	0.169	182	204	203	256
1393.871	0.459	0.180	156	198	131	187
3538.894	0.799	0.394	164	179	177	132
3541.890	0.955	0.425	174	179	174	183
3561.877	0.993	0.632	161	167	177	170
3576.795	0.768	0.787	146	143	139	102
3635.520	0.815	0.395	176	183	167	. . .
3638.763	0.984	0.428	162	185	296	162
3641.662	0.134	0.458	169	167	171	137
3665.527	0.373	0.706	151	162	174	114
3715.789	0.982	0.226	211	202	204	. . .
3716.539	0.021	0.234	186	182	183	164
3731.539	0.799	0.389	192	179	173	. . .
3735.551	0.007	0.431	184	183	180	199
3738.539	0.163	0.462	170	177	181	169

Little can be said at this time regarding the nature of the secondary component of the *Star C* system. There is marginal evidence for the presence of weak absorptions that may move

---

[12] The 1998–1999 data are RVs measured on the same spectra that were used by Schweickhardt (2000).

[13] Schweickhardt searched for modulation on the $P_{\rm AB}$ period in the O III 5592 photospheric absorption RVs and convincingly showed that it was not present.

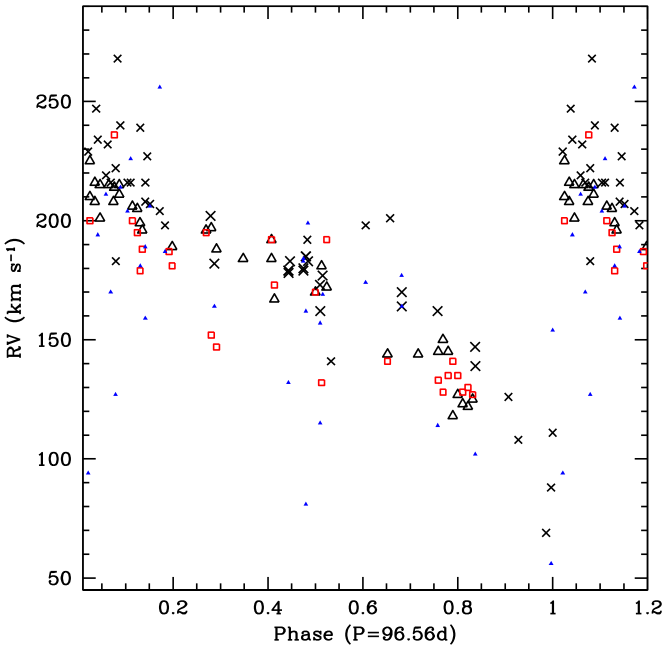

Figure 7. RV measurements of the *Star C* lines plotted against phase computed with $P_C = 96.56$ days. Open triangles (LCO spectra) and crosses (FEROS spectra) correspond to the photospheric absorptions of O III and He I; open squares (LCO) and filled-in triangles (FEROS) correspond to the weak C III 5696 emission line.

(A color version of this figure is available in the online journal.)

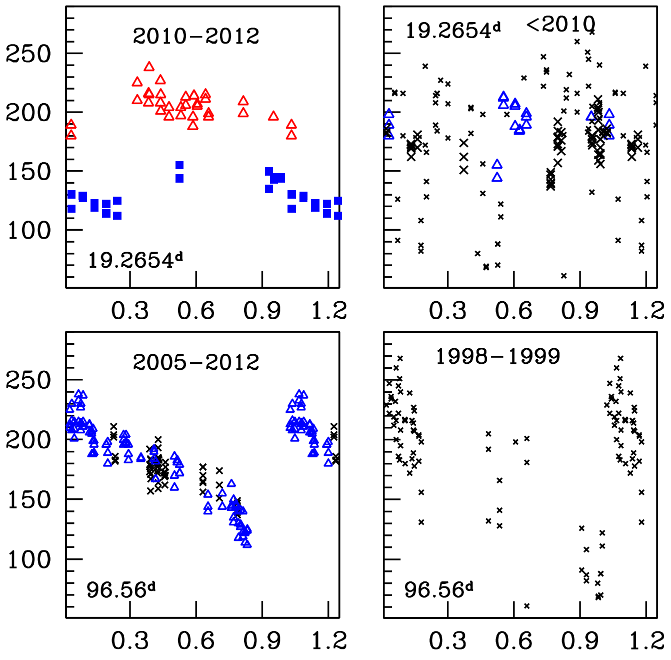

Figure 8. RVs of the photospheric absorption lines O III 5592 and He I 4471, 5875 Å plotted as a function of phase computed with $P = 19.2654$ days (top) and 96.56 days (bottom) for different epochs of observation. The apparent modulation of the 2010–2012 data on the 19.2654 day period is due to a chance coincidence: open triangles and filled squares indicate, respectively, data with $\phi_C = 0.0$–0.3 and 0.7–1.0, phase ranges at which maximum and minimum of the 96.56 day modulation occur.

(A color version of this figure is available in the online journal.)

in anti-phase with the primary lines as illustrated in Figure 9. Significantly higher S/N spectra are required for further analysis of this issue, however.

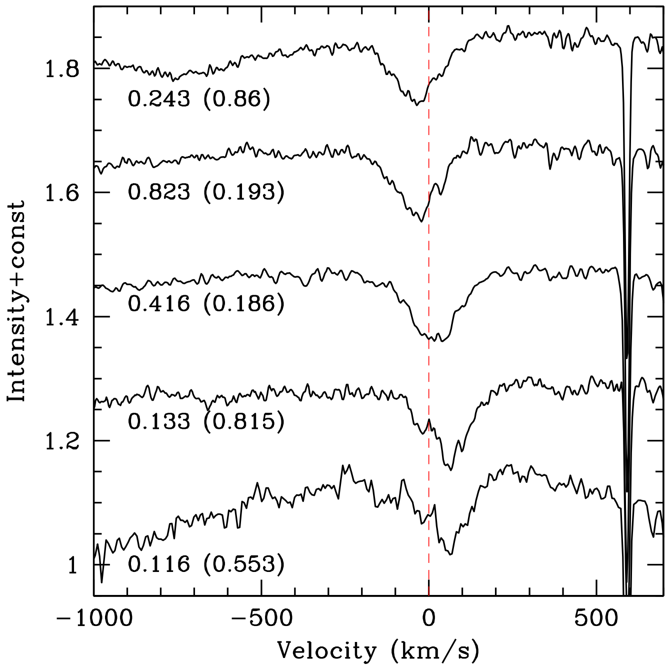

Figure 9. He I 5875 Å photospheric absorption plotted on a velocity scale corrected for +150 km s^{-1} SMC motion and displaced vertically in order of increasing phase on the 96.56 day period. The shift in the absorption minimum is consistent with orbital motion of the primary component of *Star C*, and there is marginal evidence for the presence of a weaker absorption moving in anti-phase which, if confirmed, would correspond to the secondary component. Listed are the phases for the 96.56 day period and, in parentheses, the phases corresponding to the 19.3 day period.

(A color version of this figure is available in the online journal.)

Finally, we note that the RVs of the weak C III 5696 Å emission line follow the same trend as the photospheric absorptions and thus it originates in *Star C*.

5. ORBITAL SOLUTIONS

5.1. *The 19.3* Day *WR/LBV System*

We employed the FOTEL[14] program (Hadrava 2004) to fit the RV variations of the two Doppler-shifted emission lines of N V 4944. Assigning the same weight to all the data points and fixing $i = 86°$ from Perrier et al. (2009), the best solution gives $M_A = 61 \pm 10\,M_\odot$, $M_B = 66 \pm 10\,M_\odot$, where the uncertainties refer to the goodness of fit. Our value for the eccentricity $e = 0.27 \pm 0.02$ is slightly smaller than that derived by Perrier et al. (2009) from the solution of the light curve ($e_{\rm Perrier} = 0.314 \pm 0.007$) but coincides with that obtained by Schweickhardt (2000) from the RV curve solution of the 1998–1999 FEROS data, $e = 0.284$. Our argument of periastron $\omega = 134\,° \pm 4$ coincides within the uncertainties with those of Perrier et al. (2009) and Schweickhardt (2000).

The FOTEL fit yields a period $P = 19.2656 \pm 0.0008$ days which coincides within the uncertainties with that derived by Sterken & Breysacher (1997), $P_{\rm AB} = 19.2654$ days. Hence, we continue to adopt the Sterken & Breysacher (1997) ephemeris in this paper. Our results do not change if the period is fixed to this value. The time of periastron that is found by our fit, HJD2,451,424.97 ± 0.25, corresponds to orbital phase $\phi_{\rm peri} = 0.075$.

---

[14] http://www.asu.cas.cz/~had/paifotel.pdf

Table 6
Orbital Solutions for *Stars A* and *B*

Element	N v 4944 RVs		System A+B
	Star A	Star B	
$M \sin^3 i$ ($M_\odot$)	61 (10)	66 (10)	127 (14)
$a \sin i$ ($R_\odot$)	78 (3)	73 (3)	151 (4)
K (km s^{-1})	214 (6)	200 (6)	...
e	...	...	0.27 (0.02)
$\omega_{\rm per}$ (deg)	...	...	134 (4)
V_0 (km s^{-1})	...	...	131 (3)
$P_{\rm calc}$ (days)	...	...	19.2656 (0.0009)
$T_{\rm peri}$ (HJD)	...	...	2451424.97 (0.25)
i°	...	...	86 (fixed)
T_0 (HJD)	...	...	2443158.71 (fixed)
$P_{\rm AB}$ (days)	...	...	19.2654 (fixed)

The parameters for the *Star A* and *Star B* system are listed in Table 6. The predicted RV curves are plotted in Figure 4, displaced by -20 km s^{-1}, consistent with an expected systematic blueshift in N v 4944 Å due to occultation by the stellar core of the wind that is receding from the observer. Our mass determination is consistent with the estimate derived in Foellmi et al. (2008), but it is larger than that of Niemela (1988) and our M_A is significantly smaller than the 90 $M_\odot$ estimated by Georgiev et al. (2011).

Niemela (1988) used the RV curves of the emission lines N v 4603 Å and N iv 4058 Å assumed to arise, respectively, from *Star A* and *Star B*. This explains the somewhat smaller masses because the N v line is affected by the P Cygni absorption component of the neighboring N v 4620 Å line while the N iv emission contains a contribution also from *Star A*.

An answer to the question of whether the 90 $M_\odot$ deduced by Georgiev et al. (2011) can be reconciled with our current results is less straightforward. The spectroscopic mass in the CMFGEN model is based on the estimated luminosity and the proximity of the star to the Eddington limit. For the 2009 model, *Star A* has $L_{\rm Edd}/L = 0.50$. If we were to use 0.6 as an upper limit for the Eddington ratio, we would obtain $M_A = 75\ M_\odot$, in better agreement with that deduced from the RV measurements. With $L_{\rm Edd}/L \geqslant 0.60$ it becomes difficult to construct a photospheric model since the radiation force will potentially exceed gravity below the photosphere because of the additional opacity due to iron (as we will discuss below; see Figure 14). However, in this regime there are radiation instabilities that need to be addressed, and clumping can potentially reduce the effective opacity (e.g., Shaviv 2001a, 2001b).

Part of the discrepancy could also arise from the deduced luminosity since the deduced spectroscopic mass scales with L. If the error in T_* is ~3% (2000 K for $T_* = 60{,}000$ K) the error in L is approximately 10%. Given the additional uncertainties arising from the spectroscopic decomposition an error in L of 20% is not unreasonable, and this translates to an error of almost 20 $M_\odot$.

Finally, we note that the uncertainty in the mass determinations quoted in Table 6 does not include the uncertainties derived from possible contributions to the N v 4944 Å emission lines arising in, for example, the WWC region, a point that will be discussed in Section 5.3.

5.2. The 96.56 Day Binary System

The RVs of the O iii 5592 and He i 4471, 5875 Å photospheric absorptions were also analyzed with the FOTEL program (Hadrava 2004), from which the following orbital elements were derived: $P_C = 96.56$ days, $e = 0.82$, $\omega = 252°$, and a time of periastron HJD2,451,183.40. As shown in Table 7, these values are consistent with those obtained by Schweickhardt (2000).

Table 7
Orbital Solution for *Star C*

Element	Current Analysis	Schweickhardt (2000)
P_C (days)	96.56 (0.01)	96.5
$T_{\rm peri}$ (HJD)	2451183.40 (0.22)	2451183.3
e	0.815 (0.020)	0.82
ω (deg)	252 (3.3)	248
K (km s^{-1})	81 (4)	76

The systemic velocity that is derived from the average of the different data sets (LCO, FEROS, three different lines) is $V_0^C = 164 \pm 5$ km s^{-1}. This is in contrast with the value we find for Stars *A* and *B*, $V_0^{\rm AB} = 131 \pm 3$ km s^{-1}. However, as pointed out above, a systematic blue shift in the N v 4944 Å emission line is expected, so once the -20 km s^{-1} estimated shift is contemplated, the value of $V_0^{\rm AB}$ is very similar to that of V_0^C, consistent with both binary systems lying at the same location within the SMC.

5.3. Do the Emission Lines Reflect Orbital Motion?

The basic assumption that is made when using spectral lines to determine the orbital parameters of a binary star is that these lines have a constant shape over the orbital cycle. In the case of an emission-line star, this translates into the assumption that the distribution of emitting atoms in the material surrounding the star is symmetric and remains constant over the orbital cycle as viewed in the frame of the observer. If these conditions are not met, then the shape of the line profiles will change over orbital phase, thus introducing a systematic deviation in the RV measurements with respect to those that yield orbital motion.

The issue of where in the HD 5980 system the emission lines are formed has been a long-standing topic of debate and has limited the efforts to determine the masses of *Star A* and *Star B*. Moffat et al. (1998) and Breysacher & François (2000) speculated that the bulk of the emission lines arises not in the stellar winds, but in the shock cone region where the two winds collide (henceforth referred to as the WWC). If this were the case, then the RV variations would describe the velocity structure along the shock cone walls, projected along the line of sight to the observer, and their use for deducing the stellar masses would be very limited.

Although the WWC shock walls may indeed give rise to emission lines, there are additional effects that may also distort the emission-line profiles. For example, the wind region belonging to the star with the weaker wind that is enclosed by the WWC constitutes a “hole” in the spherical distribution of the stronger wind star. It has been shown that this effect results in weaker emission at particular wavelength intervals that change with orbital phase (Georgiev & Koenigsberger 2004). Another interaction effect is the irradiation of *Star A*’s wind by *Star B*, which may alter the ionization and velocity structure (Gayley et al. 1997) on the affected hemisphere. One-dimensional model calculations of the P V line profile variations in *FUSE* spectra led to the conclusion that the wind structure of *Star A* is different on the hemisphere facing the companion from that of the opposite hemisphere (Koenigsberger et al. 2006), supporting this scenario.

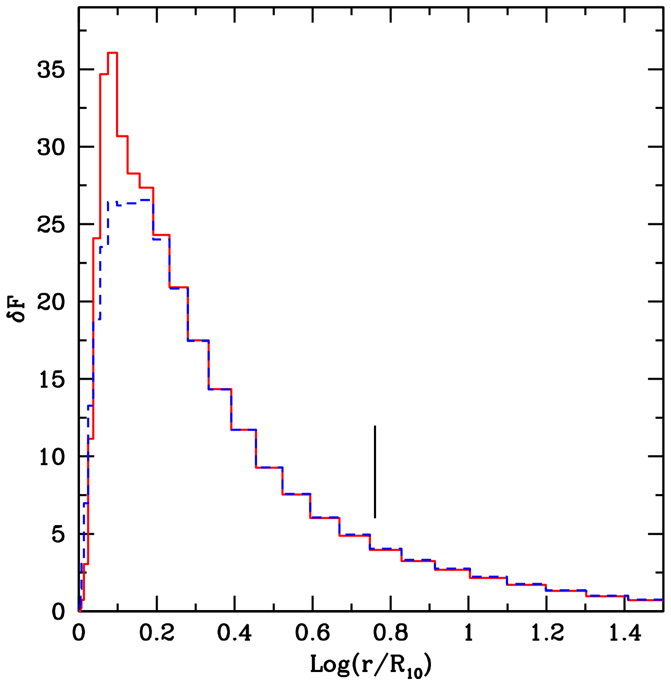

Figure 10. Shown (red, solid) is the radial contribution to the flux (N v 4994 Å line and underlying continuum) measured over a band extending from 4942.3 to 4945.3 Å. Also shown (blue, broken) is the radial contribution to the continuum flux near the N v 4994 line. These data were obtained from the CMFGEN model constructed for *Star A* for the 2009 epoch (Georgiev et al. 2011). The radius variable is given in units of $R_{10} = 19.3\ R_\odot$, which corresponds to the location where the continuum optical depth $\tau_{\rm Ross} = 10$. Adopting the orbital elements listed in Table 6, the separation between *Stars A* and *B* at periastron is $\log(R_{\rm per}/R_{10}) = 0.76$ (indicated by vertical line), which is outside of the wind region where this N v line primarily forms.

(A color version of this figure is available in the online journal.)

Although a proper analysis of irradiation, WWC, and asymmetric wind structures requires the use of two- or three-dimensional non-LTE radiative transfer computations, the dominant effect of these interaction effects is expected to be present in the outer wind regions. Hence, as we shall argue below, emission lines that are formed in the innermost wind regions, such as N v 4944 Å, are likely to be much less affected.

Weak emission lines such as N v 4944 Å are formed in a small volume, one that is comparable to that of the continuum forming region, as we illustrate in Figure 10 which shows the extent of the N v 4944 Å forming region computed by the CMFGEN model for *Star A* (Georgiev et al. 2011). The bulk of this emission arises at $\log(r/R_{10}) \leqslant 0.3$, where R_{10} is the radius at which the continuum optical depth τ is 10. Adopting $R_{10} = 19.3\ R_\odot$ from Georgiev et al. (2011), we find that the bulk of the N v 4944 Å is formed at $<40\ R_\odot$, which is significantly smaller than the orbital separation, even at periastron passage ($r^{\rm peri} \sim 110\ R_\odot$). This supports the assumption that the RV curve of this N v line is likely to be unperturbed by interaction effects.

A further test is to compare the CMFGEN model line profiles with the observations, for which we synthesized spectra of the HD 5980 system under the following conditions: (1) the relative continuum brightnesses of *Star A*, *B*, and *C* in the visual spectral region are, respectively, 40%, 30%, and 30%; (2) the emission-line spectrum of *Star B* is approximated with the CMFGEN emission-line spectrum of *Star A* computed by Georgiev et al. (2011) for the 2009 epoch, scaled to the relative luminosity of *Star B*; (3) the spectrum of *Star C* is represented by the appropriate CMFGEN model (Georgiev et al. 2011).

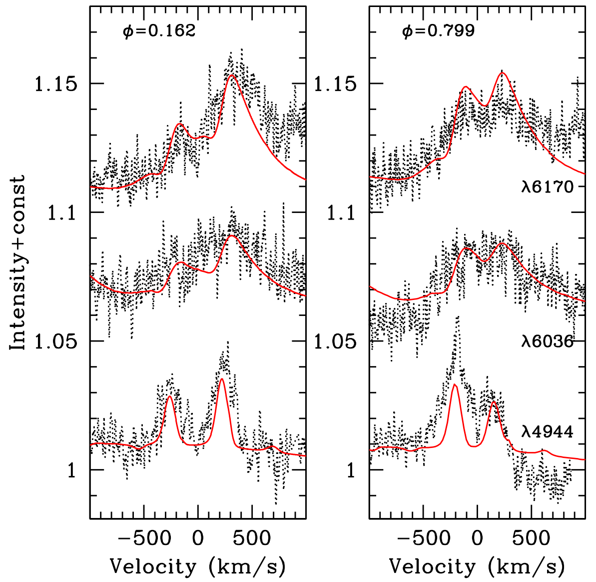

Figure 11. Comparison of FEROS spectra (dots) obtained at two orbital phases with the synthetic spectrum constructed for the HD 5980 system using the CMFGEN model computed for *Star A* and *Star C* by Georgiev et al. (2011) and assuming that *Star B*'s spectrum is similar to that of *Star A*. The velocity scale is centered on the laboratory wavelength of N v 4944 Å and He ii 6036 and 6170 Å.

(A color version of this figure is available in the online journal.)

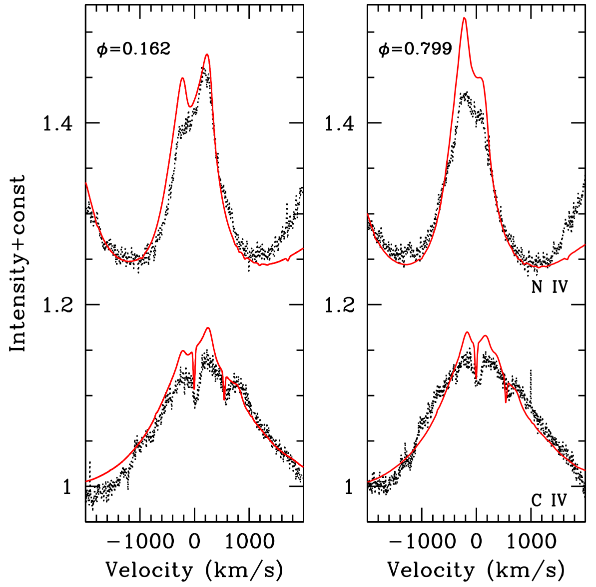

Figure 12. Same as Figure 11 but here the velocity scale is centered on the laboratory wavelength of C iv 5801 Å (left) and N iv 4058 Å (right).

(A color version of this figure is available in the online journal.)

The CMFGEN model spectra for *Star A* and *Star B* were Doppler-shifted to the RVs measured on the N v 4944 Å line in the FEROS spectra at orbital phases $\phi = 0.162$ and 0.799. These were then combined with each other and with the spectrum of *Star C* to create the synthetic spectrum of the triple system at these two orbital phases.

Figures 11 and 12 present a selection of emission-line profiles in the spectra obtained in the year 2006 at orbital phases $\phi = 0.162$ (left panel) and $\phi = 0.799$ (right panel) compared with the synthetic spectrum computed for the corresponding phases. Other than the discrepancies in line strengths which are to be expected given the uncertainties in the input parameters for the CMFGEN model, the synthetic triple-star spectrum reproduces quite well the observations. Hence, there is no indication that the lines shown in these figures are affected in any significant way by the interaction effects in the binary system.

It is also important to note that the N v 4944 Å emission at orbital phase $\phi = 0.162$ consists of two *separate* lines, both of which reach the local continuum level; i.e., they are not really "double peaked" emission lines, a shape predicted from models of emission arising in the WWC shock cone walls (see, for example, Henley et al. 2003).

Finally, we note that although winds with similar momentum ratios lead to a WWC region in which the phase-dependence of emission line profiles is similar to that of two distinct wind sources, to the extent of our knowledge, no calculation of the intensity of such emission lines has been performed. Thus, it is not possible to assess the relative importance of this emission compared to that which arises from the inner wind regions of the two stars.

Hence, we conclude that, given the information for HD 5980 that is available at this time and given the lack of models that predict the strength of the emission lines expected to arise in a WWC region, the assumption that the N v 4944 Å emission line arises primarily in the inner stellar winds of the stars is a sound one.

Clearly, however, this conclusion is based on the premise that *Star B* possesses an emission-line spectrum that arises in a high-ionization stellar wind typical of WNE-type stars. This premise is based on observations obtained prior to and during the eruptive state (Breysacher et al. 1982; Niemela 1988; Koenigsberger 2004). If *Star B* were to be a non-WR star, then the WNE-type spectrum that has been observed for >60 yr would have to arise entirely in *Star A* and, potentially, in the WWC region, and the conclusions of this paper would have to be re-assessed. It is important to note, however, that the wind momentum ratio under these circumstances would most likely be such that the WWC shock cone would be folded around *Star B* and hence, a highly blueshifted emission component would be observed in lines of He I and He II near the conjunction when this star is between us and its companion,[15] something that is not observed.

6. EVOLUTIONARY STATUS

In this section we will examine the evolutionary scenarios that lead to a system such as the 19.3 day binary in HD 5980.

A preliminary examination (Koenigsberger 2004) indicated that the luminosity and effective temperature of *Star A* place it on the Hertzsprung–Russell diagram (HRD) along the evolutionary track of a 120 $M_\odot$ zero-age main sequence (ZAMS) star at an age of ~3 Myr. This is very close to the age of the NGC 346 cluster (Mokiem et al. 2006), which would indicate that such a massive star is near the final evolutionary phases leading up to an SN event. A similar result is reached if we use the most recently available grid of models for the SMC metallicity (Georgy et al. 2013). Specifically, *Star A*'s luminosity corresponds to that of a non-rotating 120 $M_\odot$ ZAMS model near the end of core helium burning at an age of 2.952 Myr or to that of a 85 $M_\odot$ model with initial rotation velocity of 400 km s^{-1} at an age of 3.63 Myr. However, both of these models predict a large increase in radius prior to these ages. Since the current Roche-lobe radius is only ~57 $R_\odot$, the interaction with the companion would have modified the subsequent evolution from that predicted by the single-star models. Thus, HD 5980 needs to be analyzed within the context of binary evolution or within scenarios in which the large radius increase in post-main sequence stages can be avoided.

The classical binary scenarios involve the assumption that a star evolves as a single star until its radius reaches some critical value, assumed to be the Roche radius. At this point in the evolution, the nature of the close companion becomes a crucial element of the analysis because it determines whether conservative or non-conservative mass transfer takes place. Our results indicate that the mass of *Star B* is close to that of *Star A* and that it, too, has a very large surface He-abundance enrichment. This excludes the conservative mass transfer scenario which requires rather similar masses initially, and thus leads to large mass ratios after the Roche lobe overflow (RLO) phase (Wellstein & Langer 1999). Non-conservative interaction, on the other hand, as expected for relatively large initial mass ratios (Petrovic et al. 2005), could leave two similar mass objects after the envelope of the initially more massive star is stripped. However, the initially less massive star would still be relatively unevolved at this time, in contrast with the rather evolved state of both stars in HD 5980. Hence, the classical binary evolution scenarios cannot readily explain the parameters of HD 5980.

The question then remains whether it is possible to avoid the large radius increase in the post-MS evolutionary stages, thus avoiding the problem of mass transfer in the system, but at the same time enhancing the surface chemical composition.

Rotational mixing brings the helium and nitrogen produced in the core efficiently to the stellar surface, thereby enriching the visible surface chemical abundances without the need of stripping large amounts of mass from these outer layers. Since this rapid rotation greatly reduces the chemical gradients present in slower rotating stars, these stars undergo what is referred to as quasi-chemically homogeneous evolution (QCHE). An important characteristic of these models is that *both* L and T increase with time, and the star remains relatively compact, thus avoiding a RLO phase. According to Brott et al. (2011), stars with rotational velocities above ~300 km s^{-1} are at the threshold for QCHE at SMC metallicity.

We computed a model binary system with initial masses 90 $M_\odot$ (Primary) and 80 $M_\odot$ (Secondary), rotational velocity $v_{\rm ini} = 500$ km s^{-1}, and orbital period of 12 days using the Binary Evolutionary Code (Heger et al. 2000; Petrovic et al. 2005; Yoon et al. 2006). For the early evolutionary stage, the prescription of Vink et al. (2001) for the mass-loss rate was adopted and for the WR stage we used the prescription of Hamann et al. (1995), with the correction of Vink & de Koter (2005) to account for the SMC metallicity. Because of the angular momentum loss due to the stellar winds, the orbital separation grows with time. After ~3.1 Myr, the binary has an orbital period of 19.2 days and the stars have each $M = 67\ M_\odot$, $\log(L/L_\odot) \sim 6.3$, highly enhanced surface He-abundances, and current surface temperatures of 63 kK, similar to the properties of *Star A* and *Star B*. More importantly, the evolution of these QCHE model stars places them on the HRD at systematically higher temperatures and luminosities, as shown in Figure 13, without any large radius increases that would lead to mass transfer.

The other parameters of the QCHE model stars are listed in Table 8, along with the corresponding values for *Star A*. Since the Secondary is the originally less massive member of the binary system, it evolves slower than the companion and

---

[15] See illustrations of a similar geometries in Figures 20–22 of Koenigsberger (2004).

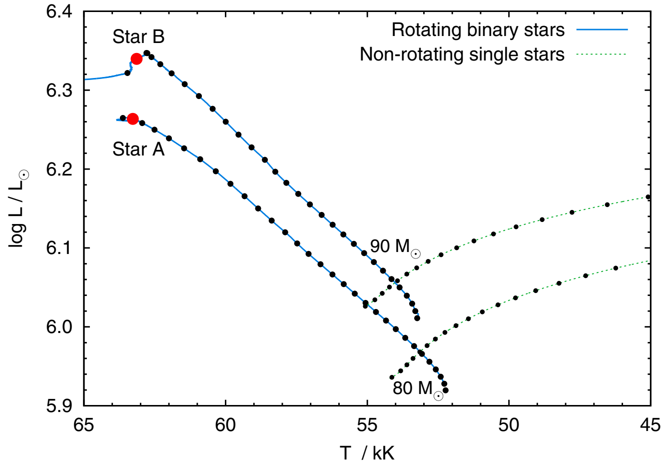

Figure 13. Hertzsprung–Russell diagram (HRD) of our binary model with an initial orbital period of 12 days, initial surface rotational velocity $v_{\rm ini} = 500$ km s^{-1}, and initial masses of 90 $M_\odot$ and 80 $M_\odot$, compared for reference to the evolution of same mass non-rotating stars. Black dots are shown every 0.1 Myr. The red circles indicate the position of the two HD 5980 binary components after ∼3.1 Myr, which is when their surface properties agree best with those of *Star A* and *Star B*.

(A color version of this figure is available in the online journal.)

Table 8
Binary Evolution Model[a]

Parameter	Primary	Secondary	*Star A*	Notes[b]
Age (Myr)	3.1	3.1	∼3	1
$M_{\rm ZAMS}$ ($M_\odot$)	90	80	. . .	. . .
M ($M_\odot$)	67	67	51–71	this paper
$P_{\rm orb}$ (days)	19.2	19.2	19.26	
$\log(L/L_\odot)$	6.34	6.26	6.39	3
Y	0.92	0.84	0.80	3, 4
$T_{\rm phot}$ (kK)	63.0	63.0	60	3
$v_{\rm surf}$	195	257	250:	2
$R_{\rm phot}$ ($R_\odot$)	12.5	11.3	19–24	5
$\dot{M}(10^{-5} M_\odot$ yr^{-1})	5.5	3.1	3.6	3

Notes.

[a] The computed model is with initial orbital period of 12 days, surface rotational velocity $v_{\rm ini} = 500$ km s^{-1}, and metallicity $Z = 0.0021$. $v_{\rm surf}$ is the surface rotation velocity.

[b] References for Columns 2 and 3: (1) Mokiem et al. 2006; (2) Georgiev & Koenigsberger 2004; (3) Georgiev et al. 2011; (4) Koenigsberger et al. 1998; (5) Perrier et al. 2009.

thus corresponds to *Star A*, so the comparison to be made is between *Star A*'s observationally derived parameters and those of the secondary in the QCHE model. The mass-loss rate of *Star A* in 2009 is listed by Georgiev et al. (2011) as $\dot{M}/\sqrt(f) = 23\times10^{-5}$ $M_\odot$ yr^{-1}, and they adopt a wind "clumping" factor $f = 0.025$. Hence, $\dot{M}_A = 3.6\times10^{-5}$ $M_\odot$ yr^{-1}, which is very similar to that of the Secondary in the QCHE model.

Although there is no direct means of determining the surface rotation velocity of the WR-type stars in HD 5980, Georgiev & Koenigsberger (2004) speculated that the low-amplitude modulation of *Star C*'s photospheric absorptions that was reported in early observational data by Breysacher et al. (1982) could be caused by a much larger amplitude Doppler shift of underlying broad lines which, due to their width, would not be detectable in the HD 5980 spectrum. Under this assumption, they found that the possible absorption lines would correspond to *Star A* rotation speeds of $v \sin i \sim 200$–250 km s^{-1}, which is of the order of the rotation predicted for the Secondary in the QCHE model.

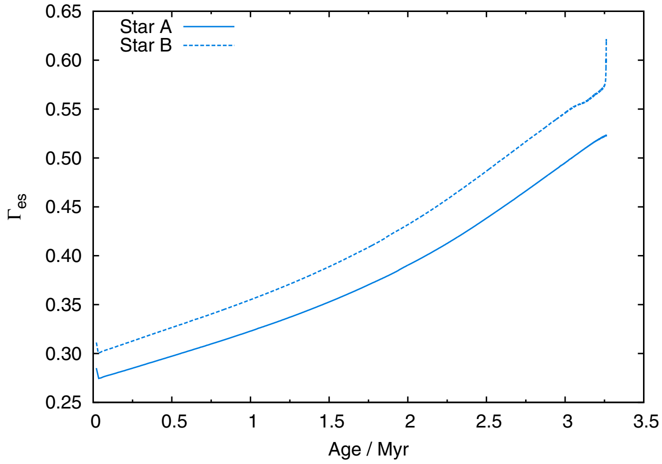

Figure 14. Value of the electron scattering Eddington factor over time since arriving at the main sequence showing its systematic increase.

(A color version of this figure is available in the online journal.)

The final point to note concerns the predicted radii of the QCHE model stars, $R_{\rm Prim} = 12.5\,R_\odot$ and $R_{\rm Sec} = 11.3\,R_\odot$. The analysis of the optical eclipse light curve of HD 5980 (Perrier et al. 2009) yielded relative radii of $\rho_A/a = 0.158$ and $\rho_B/a = 0.108$, where a is the semi-major axis of the orbit. From Table 6, $a = 151\,R_\odot$ which implies that the occulting disks are $R_B \sim 16\,R_\odot$ and $R_A \sim 24\,R_\odot$. The latter is ∼2 times larger than predicted by the QCHE model. However, it must be considered that: (1) the derived radius for the occulting disk in WR stars depends on the wavelength of observations, with smaller wavelengths yielding smaller radii (Cherepashchuk et al. 1984), so a small correction may be viable if UV light curves are analyzed; and (2) the light curve solution of Perrier et al. (2009) is based on the assumption that only *Star B* possesses an extended optically thick wind, so it remains to be determined whether assuming that both stars have such a region would result in a smaller radius for *Star A*.

We thus conclude that a plausible scenario for the evolutionary state of the 19.3 day binary in HD 5980 is one in which both stars have followed QCHE pathways.

Furthermore, the internal luminosity structure of the QCHE models is such that therein may reside the mechanism that triggered the sudden eruption observed in 1994. The increasing luminosity over time causes an increase in the Eddington electron scattering Γ-factor (Γ_{es}), thus lowering the effective gravity at the surface. Figure 14 shows how the Γ_{es}-factor grows beyond 0.5 as the age of the star approaches that of *Star A*. This is consistent with the value of Γ_{es} found by Georgiev et al. (2011) from the spectrum of 2009. More important, however, is the fact that the *total* Γ (i.e., that computed with the total opacity, not only the electron scattering opacity) becomes larger than unity near the surface layers (Figure 15). One possible mechanism driving the eruption observed in 1994 might be related to this super-Eddington layer which might turn unstable (Humphreys & Davidson 1994; Stothers & Chin 1996). We speculate that in the case of HD 5980, the instability could have been triggered by the perturbations that arise due to its eccentric orbit. A discussion of the potential role of the companion in the case of η Car has also been discussed by Davidson (2012).

The question that then arises is whether the same mechanism could be active in other LBVs. An objection to the QCHE

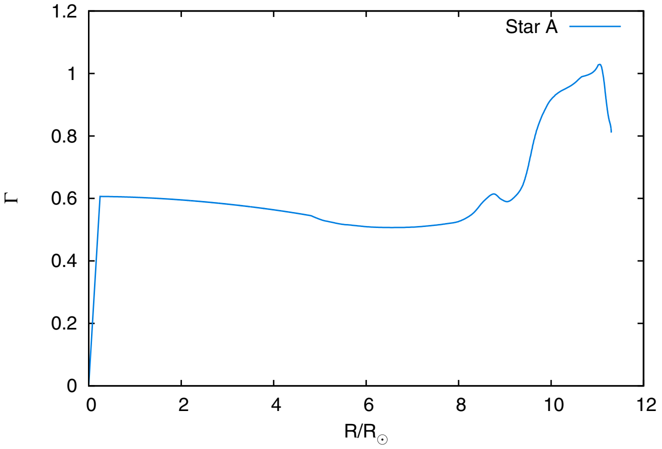

Figure 15. Value of the total Eddington factor, calculated using the total opacity (not just that due to electron scattering) and the radiative flux in *Star A* as a function of distance from stellar core. Note the super-Eddington values very close to the surface that are caused by the Fe-opacity "bump."

(A color version of this figure is available in the online journal.)

scenario is that in order for stars to follow this path, the rotation rate needs to remain high throughout their evolution, a condition that is difficult to satisfy due to the expected loss of angular momentum through stellar winds and tidal interactions. To avoid this problem, de Mink et al. (2009) suggested that very short-period, tidally locked binary systems could sustain the very rapid rotation velocities that are required. However, none of the known LBV binaries are in orbits that are close enough to meet this criterion, even after considering orbital evolution.

However, the important point to note is that for QCH evolution to take place, the star must be able to efficiently mix the nuclear processed material up to the surface layers, and rapid rotation may not be the only mechanism that can produce this effect. For example, though speculative at this time, an alternative to rapid rotation for efficient mixing might be the time-dependent velocity field that is driven by the tidal interactions in an asynchronously rotating binary star (Koenigsberger & Moreno 2013). With this mechanism, one could start out with a relatively wider binary than is required by the fast-rotation models and, as long as the stellar rotation remains asynchronous, the induced velocity field could contribute toward the mixing processes. Whether the efficiency with which the mixing occurs is sufficient for QCHE to be attained, however, remains to be proven.

Little can be said at this time about the evolutionary status of the *Star C* binary except for noting that such highly eccentric binary systems are rarely found in orbits with periods shorter than 100 days, which suggests that it may be gravitationally bound to the *Star A* + *Star B* pair. The 5:1 resonance in the orbital periods of the two systems is further evidence in support of this hypothesis. In triple hierarchical systems, the outer period tends to be a multiple of the inner binary period, as in σ Ori (Aa+Ab) + B (Simón-Díaz et al. 2011). If a similar condition were to hold in HD 5980, then both P_{AB} and P_C would be sub-multiples of the outer period and hence, would be related to each other, as observed. Thus, we speculate that the *Star C* components have a similar age as *Star A* and *Star B*.

7. CONCLUSIONS

Due to their short lifetime, LBVs are quite rare and most of them are apparently single objects, impeding a direct determination of their current mass. Determining basic parameters for the LBVs undergoing major eruptions is even more challenging, since the majority are detected only in distant galaxies and little or no information exists on the properties of the star prior to the eruptive event.

In this context, the importance of HD 5980 for understanding massive star evolution cannot be overstated. It provides the closest and clearest example of mass-loss phenomena during the short-lived LBV and WR phases in low-metallicity star forming regions such as those where the most distant LBV events are being observed and which, in addition, host the brightest gamma-ray events. Furthermore, massive objects such as those in HD 5980 are believed to be the progenitors of some of these events.

The following are the conclusions of this paper.

1. The masses in the 19.3 day *Star A*+*Star B* system have been constrained under the premise that both stars currently possess a WNE-type spectrum. The largest uncertainties in this determination derive from: a) the fact that the spectrum of *Star B* has not been unambiguously isolated from that of *Star A*; and b) the lack of detailed models predicting the strength of the emission lines that can arise in the WWC region.
2. A plausible scenario for the evolutionary state of the 19.3 day binary in HD 5980 is one in which both stars have followed a quasi-chemically homogeneous evolutionary path. We speculate that the high mixing efficiency that is required may be provided, at least in part, by the non-uniform differential rotation structure that is driven by the tidal forces in an asynchronously rotating binary star. HD 5980 may thus be the first binary system which provides evidence that QCHE can indeed occur, since it possesses the two extreme properties that are required for this scenario, i.e., a very high mass of its components, and a very low metallicity. If confirmed this would imply that both stars in HD 5980 can be considered as candidates for gamma-ray burst progenitors (Yoon et al. 2006) or even pair instability SNe (Langer et al. 2007).
3. The instability that caused the 1994 eruption may be related to the super-Eddington layer which is present just below the photosphere in the QCHE models.
4. A 96.5 day period is confirmed for the RV variations of the photospheric absorptions arising in the third component, *Star C*, indicating that this star is also a binary. We point out that this period is in a 5:1 ratio with the period of the *Star A* + *Star B* binary, suggesting that these four stars may constitute a hierarchical quadruple system.

We dedicate this paper to the memory of our friends and colleagues Virpi Niemela and Leonid Georgiev.

We thank Sylvia Ekstrom for providing the SMC evolutionary models in advance of publication and Ulises Amaya and Francisco Ruíz Salazar for computer support. G.K. acknowledges UNAM/PAPIIT grant IN 105313 and CONACYT grant 129343. R.H.B. acknowledges support from FONDECYT Regular Project 1140076. D.J.H. acknowledges support from Grant HST-GO-11623.01-A. The *HST* is operated by STScI under contract with AURA. We thank Eric Hsiao (Carnegie Supernova Project) and Josh Simon for the MIKE spectrum of 2012 June 6; and Ricardo Covarrubias for the 2007 August 30 MIKE spectrum taken during Clay engineering time. We are indebted to the Carnegie TAC for generous observing time allocation at the du Pont telescope, and to the authorities of Las Campanas for offering us the opportunity to observe at du Pont during engineering time in 2013 July.

REFERENCES

Barbá, R. H., Morrell, N. I., Niemela, V. S., et al. 1996, Rev. Mex. Astron. Astrofis. Conf. Ser., 5, 85

Breysacher, J., & François, P. 2000, A&A, 361, 231

Breysacher, J., Moffat, A. F. J., & Niemela, V. 1982, ApJ, 257, 116

Breysacher, J., & Perrier, C. 1991, in IAU Symp. 143, Wolf Rayet Stars and Interrelations with Other Massive Stars in Galaxies, ed. K. van der Hucht & B. Hidayat (Dordrecht: Kluwer), 229 (BP91)

Brott, I., de Mink, S. E., Cantiello, M., et al. 2011, A&A, 530, 115

Cherepashchuk, A. M., Eaton, J. A., & Khaliullin, Kh. F. 1984, ApJ, 281, 774

Davidson, K. 2012, in Eta Carinae and the Supernova Impostors, ed. K. Davidson & R. M. Humphreys (New York: Springer), 43

de Mink, S., Cantiello, M., Langer, N., et al. 2009, A&A, 497, 243

Foellmi, C., Koenigsberger, G., Georgiev, L., et al. 2008, RMxAA, 44, 3

Gayley, K. G., Owocki, S. P., & Cranmer, S. R. 1997, ApJ, 475, 786

Georgiev, L., & Koenigsberger, G. 2004, in IAU Symp. 215, Stellar Rotation, ed. A. Maeder & P. Eenens (San Francisco, CA: ASP), 111

Georgiev, L., Koenigsberger, G., Hillier, J. D., et al. 2011, AJ, 142, 191

Georgy, C., Ekström, S., Eggenberger, P., et al. 2013, A&A, 558, 103

Hadrava, P. 2004, Publ. Astron. Inst. ASCR, 92, 1

Hamann, W.-R., Koesterke, L., & Wessolowski, U. 1995, A&A, 299, 151

Heger, A., Langer, N., & Woosley, S. E. 2000, ApJ, 528, 368

Henley, D. B., Stevens, I. R., & Pittard, J. M. 2003, MNRAS, 346, 773

Humphreys, R. M., & Davidson, K. 1994, PASP, 106, 1025

Kaufer, A., Schmid, H. M., Schweickhardt, J., & Tubbesing, S. 2002, in ASP Conf. Ser. 260, Interacting Winds from Massive Stars, ed. A. F. J. Moffat & N. St-Louis (San Francisco, CA: ASP), 489

Koenigsberger, G. 2004, RMxAA, 40, 107

Koenigsberger, G., Auer, L. H., Georgiev, L., & Guinan, E. 1998, ApJ, 496, 934

Koenigsberger, G., Fullerton, A., Massa, D., & Auer, L. H. 2006, AJ, 132, 1527

Koenigsberger, G., Georgiev, L., Hillier, D. J., et al. 2010, AJ, 139, 2600

Koenigsberger, G., Kurucz, R., & Georgiev, L. 2002, ApJ, 581, 598

Koenigsberger, G., & Moreno, E. 2013, in EAS Publication Series, Vol. 64, ed. A. Tkachenko & K. Pavlovski (Cambridge: Cambridge Univ. Press), 339

Langer, N. 2012, ARA&A, 50, 107

Langer, N., Hamann, W.-R., Lennon, M., et al. 1994, A&A, 290, 819

Langer, N., Norman, C. A., de Koter, A., et al. 2007, A&A, 475, 19

Maeder, A., & Meynet, G. 1987, A&A, 182, 243

Moffat, A. F. J., Marchenko, S. V., Bartzakos, P., et al. 1998, ApJ, 497, 896

Mokiem, M. R., de Koter, A., Evans, C. J., et al. 2006, A&A, 456, 1131

Niemela, V. S 1988, in ASP Conf. Ser. 1, Progress and Opportunities in Southern Hemisphere Optical Astronomy, ed. V. M. Blanco & M. M. Phillips (San Francisco, CA: ASP), 381

Perrier, C., Breysacher, J., & Rauw, G. 2009, A&A, 503, 963

Petrovic, J., Langer, N., Yoon, S.-C., & Heger, A. 2005, A&A, 435, 19

Schweickhardt, J., Wolf, B., Schmid, H. M., et al. 2000, in ASP Conf. Ser. 204, Thermal and Ionization Aspects of Flows from Hot Stars, ed. H. Lamers & A. Sapar (San Francisco, CA: ASP), 113

Shaviv, N. J. 2001a, ApJ, 549, 1093

Shaviv, N. J. 2001b, MNRAS, 326, 126

Simón-Díaz, S., Caballero, J. A., & Lorenzo, J. 2011, ApJ, 742, 55

Sterken, C., & Breysacher, J. 1997, A&A, 328, 269

Stothers, R. B., & Chin, C.-W. 1996, ApJ, 468, 842

Vink, J. S., Bestenlehner, J. M., Gräfener, G., de Koter, A., & Langer, N. 2012, ASPC, 465, 207

Vink, J. S., & de Koter, A. 2005, A&A, 442, 587

Vink, J. S., de Koter, A., & Lamers, H. J. G. L. M. 2001, A&A, 369, 574

Wellstein, S., & Langer, N. 1999, A&A, 350, 148

Yoon, S.-C., Langer, N., & Norman, C. 2006, A&A, 460, 199